Reynolds number dependence of drag reduction by rodlike polymers

Yacine Amarouchene,[1] Daniel Bonn,[2] Hamid Kellay,[1] Ting-Shek Lo,[3] Victor S. L'vov,[3] and Itamar Procaccia[3]
[1]*CPMOH, U. Bordeaux 1, 351 Cours de la Libération, 33405 Talence, France*
[2]*LPS, ENS, 24 Rue Lhomond, 75005 Paris, France and van der Waals-Zeeman Instituut, University of Amsterdam, Valckenierstraat 65, 1018 XE Amsterdam, The Netherlands*
[3]*Department of Chemical Physics, The Weizmann Institute of Science, Rehovot 76100, Israel*

(Received 21 December 2006; accepted 17 April 2008; published online 20 June 2008)

We present experimental and theoretical results addressing the Reynolds number (Re) dependence of drag reduction by sufficiently large concentrations of rodlike polymers in turbulent wall-bounded flows. It is shown that when Re is small the drag is *enhanced*. On the other hand, when Re increases, the drag is reduced and eventually, the maximal drag reduction asymptote is attained. The theory is shown to be in agreement with experiments, explaining the universal and rationalizing some of the the nonuniversal aspects of drag reduction by rodlike polymers. © *2008 American Institute of Physics*. [DOI: 10.1063/1.2931576]

I. INTRODUCTION

The aim of this paper is to present data and theoretical results concerning the phenomenon of turbulent drag reduction by rodlike polymers. Drag reduction implies an increase in the mean streamwise velocity (for the same pressure head) in turbulent flows as a result of the addition of tiny amounts of polymers. This implies a wide range of industrial applications and consequently, the effect, discovered in 1944 by Toms,[1] has been studied intensively over the past few decades (see, e.g., Ref. 2). The main aim of this paper is to rationalize and understand the change from drag enhancement to drag reduction by rodlike polymers in turbulent wall-bounded flows as a function of the Reynolds number Re.[3–5] To this aim, we present new experimental data and a theoretical analysis.

A classical example of the phenomenon of interest is shown in Fig. 1 which pertains to pipe flow.[4] We denote the velocity field as $\boldsymbol{U}(\boldsymbol{r},t)$ and its mean over time as $V(y)$, where y is the distance from the wall. With the mean shear defined as $S(y) \equiv dV(y)/dy$, the friction factor is defined as

$$f \equiv \tau_w \Big/ \left(\tfrac{1}{2}\rho \widetilde{V}^2\right), \tag{1}$$

where τ_w is the wall shear stress at the wall

$$\tau_w \equiv \rho \nu S(y=0), \tag{2}$$

where ν, ρ, and $\widetilde{V}$ are the kinematic viscosity, the fluid density, and the mean fluid velocity, respectively. Figure 1 presents this quantity as a function of Re in the traditional Prandtl–Kármán coordinates $1/\sqrt{f}$ versus $\mathrm{Re}_s\sqrt{f}$. Here, Re_s is the Reynolds number $\widetilde{V}L/\nu_0$, where L and ν_0 are the channel half width and the kinematic viscosity of the solvent, respectively. The straight continuous line denoted by "N" presents the Newtonian universal law. Data points below this line are indicative of a drag enhancement, i.e., an increase in the dissipation due to the addition of the polymer. Conversely, data points above the line correspond to drag reduction, which is always bound by the maximal drag reduction (MDR) asymptote represented by the dashed line denoted by "M." This figure shows data for a rodlike polymer (a polyelectrolyte in aqueous solution at very low salt concentration) and shows how drag enhancement for low values of Re crosses over to drag reduction at large values of Re.[4] One of the results of this paper is the theory that will be presented below, which reproduces the phenomena shown in Fig. 1 in a satisfactory manner.

It is interesting to note that with *flexible* polymers, the situation is very different, and there is no drag enhancement at any value of Re. The reason for this distinction will be made clear below as well. At this point, we remark that the main difference between flexible and rodlike polymers is that the former need a minimal value of Reynolds number in order to stretch (i.e., undergo the coiled-to-stretched transition, whereas rodlike polymers are "stretched" at any value of the Reynolds number. This consequence of this distinction will be further clarified below.

In Sec. II, we will present new experimental results in which drag reduction is measured as a function of the Reynolds number and for different concentrations of the rodlike polymer. We determine the rheological properties of these solutions simultaneously, so that the rheology of the solutions is known. In Sec. III, we will review the basic theoretical approach to drag reduction, in general, and by rodlike polymers, in particular. In Sec. IV, we will explain how to solve the equations and present the results and their comparison to the experiments. Discussions and the conclusions will be presented in Sec. V.

II. EXPERIMENTAL

A. Flow geometry and polymer

In this section we describe the experimental results obtained using well-characterized rodlike polymer solutions. The turbulence cell has been previously described in detail by Cadot *et al.*[6,7] A turbulent flow is generated in a closed cylindrical cell (volume of 3 l) between two counter-rotating disks spaced by one disk diameter apart. The disks are driven by dc motors. The motors are configured to keep the disks

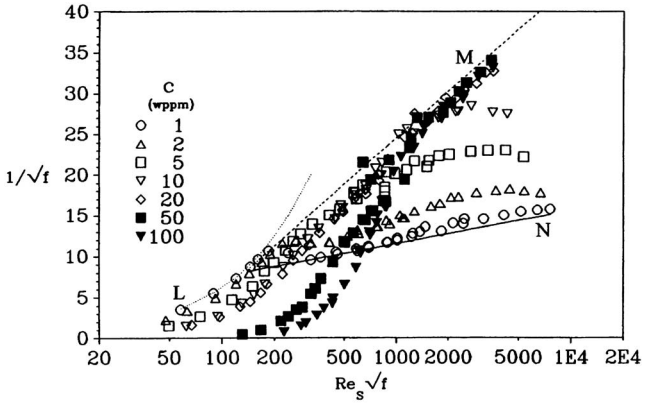

FIG. 1. The drag in Prandtl–Kármán coordinates for the water with the rodlike polymer partially hydrolyzed polyacrylamide B1120 in 0.0001N NaCl in a pipe flow (see Ref. 4 for details). The symbols represent the concentrations in wppm as given in the figure.

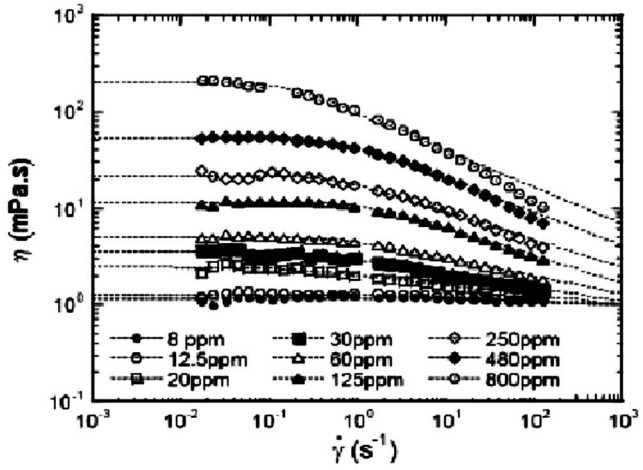

FIG. 2. Shear viscosity as a function of shear rate for various concentrations of polymers.

rotating at a constant angular velocity Ω, independently of the torque exerted by the turbulent fluid on the disks. Thus, all the experiments presented here are performed at constant angular velocity. All experiments were repeated with pure water and with the water seeded with the polymers. In both cases, we define[7] the integral Reynolds number as $\mathrm{Re}=\rho\Omega R^2/\eta_S$, where ρ is the density and R is the radius of the disks. To determine the energy dissipation in the turbulent fluid (from which we also infer the amount of drag reduction or drag enhancement), we take advantage of the fact that we are in a closed system. All the kinetic energy fed into the flow will eventually be dissipated viscously, leading to a temperature increase of the fluid: by measuring the temperature increase in time $\Delta T/\Delta t$, we can also estimate the power dissipated by the turbulent flow. The temperature is measured with a Pt thermocouple probe with an accuracy of 0.01 °C. From our temperature measurements, we can then deduce the percentage of drag reduction (DR) from

$$\mathrm{DR}(\%) \equiv 100 \times \left[1 - \frac{(\Delta T/\Delta t)_{\mathrm{poly}}}{(\Delta T/\Delta t)_{\mathrm{water}}}\right]. \tag{3}$$

For the polymer, we use solutions of xanthane, a stiff rodlike polymer with an average molecular weight $M_w=3\times10^6$ g mol^{-1}.

The rheology of the polymer solutions was studied on a Reologica Stress-Tech (cone-plate geometry) rheometer. The latter is equipped with a normal force transducer and has a large cone (55 mm) with a small angle (0.4°) in order to be able to detect small normal stress differences at high shear rates. Changing the concentration allows us to modify the shear-dependent viscosity of the solutions.[8–10] The apparent viscosity decreases with increasing shear rate; i.e., the fluid is shear thinning (Fig. 2). A satisfactory description of most of the data for high shear rates can be obtained by using the Ostwald–de Waele power law model[11] for the viscosity η: $\eta=k_1S^{(n-1)}$; the viscosity shows a power law dependence on the shear rate S. The validity of this model is limited to a certain range of shear rates, depending on the concentration C of the polymer solution; the range and constants k_1 and n are reported in Ref. 12. For the whole concentration range studied here ($0<C<2000$ wppm), no measurable normal stresses were found in the range of shear rates studied ($10<S<6000$ s^{-1}); the uncertainty on the measurements is of the order of 10 Pa.

The other important difference in the rheology of the rigid polymers, compared to solutions of flexible polymers, is the elongational viscosity η_E, which quantifies the resistance to stretching of a fluid element. If sufficiently important, η_E can be measured[13] by looking at droplet fission with a rapid camera. The dynamics of the thinning of the filament that connects the droplet to the orifice can be used to obtain the elongational viscosity, since the stretching of the filament corresponds to a perfectly elongational flow. By performing this experiment, we find that, for the rigid polymer solution, η_E is so low that the dynamics of the filament is nearly indistinguishable from that of pure water, for which $\eta_E=3$ mPa s.[14]

B. Results

In the upper panel of Fig. 3, the percentage drag reduction DR(%) is plotted as a function of the Reynolds number for three different polymer concentrations. Also, in our measurement geometry and with our rodlike polymer at low Re, a drag enhancement is observed, which smoothly transforms into a drag reduction at high Re. To verify the transition between drag enhancement and reduction, we present in the lower panel of Fig. 3 the dimensionless torque β as a function of Re including the water baseline and three different concentrations of the polymer. Finally, we present the data also in Prandtl–Kármán coordinates in Fig. 4. In this paper, we rationalize and explain the results presented in both Figs. 1 and 3. To this aim, we turn now to a review of the theory of drag reduction.

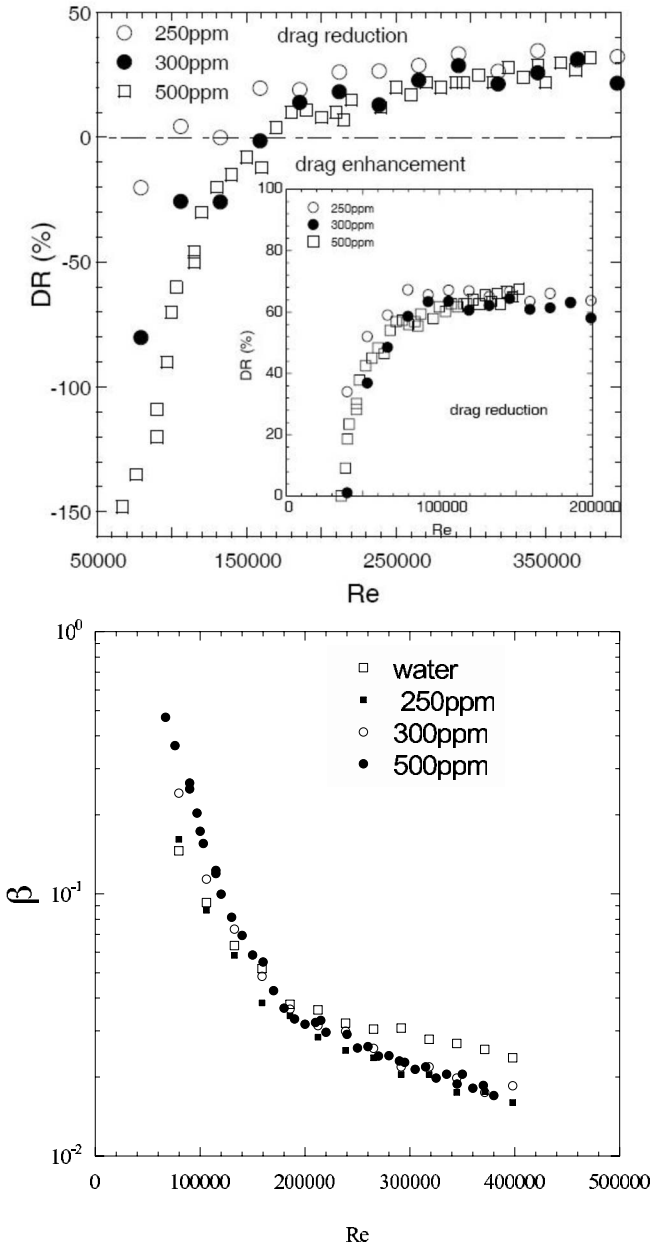

FIG. 3. Upper panel: Percentage of drag reduction (or enhancement) vs Re for three different polymer concentrations. Inset: Percentage of drag reduction vs Re when the actual viscosity (including the polymer) is used in the definition of Re. Lower panel: Dimensionless torque vs Re for water and for three concentrations of the polymer.

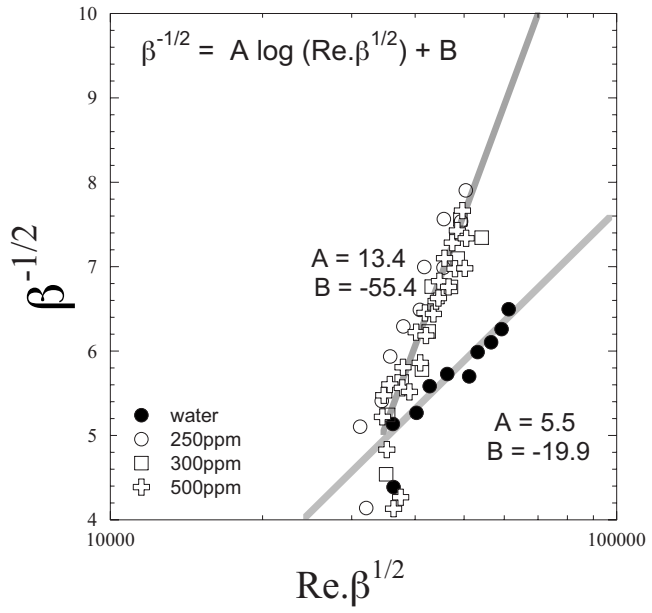

FIG. 4. Same data as in Fig. 3 but in Prandtl–Kármán coordinates.

III. REVIEW OF THE THEORY OF DRAG REDUCTION BY RODLIKE POLYMERS

In the presence of a small concentration of polymers, the Navier–Stokes equations for the fluid velocity $\boldsymbol{U}(\boldsymbol{r},t)$ gain an additional contribution to the stress tensor,

$$\frac{\partial \boldsymbol{U}}{\partial t} + \boldsymbol{U}\cdot\boldsymbol{\nabla}\boldsymbol{U} = -\nabla p + \nu_0\nabla^2\boldsymbol{U} + \nabla\cdot\boldsymbol{\sigma},$$
$$\nabla\cdot\boldsymbol{U} = 0. \tag{4}$$

The extra stress tensor $\boldsymbol{\sigma}$ is due to the interaction between the polymers and the fluid. The actual form of the stress tensor $\boldsymbol{\sigma}$ depends on whether the polymers are flexible or rodlike. The former case was dealt with frequently in literature;[15–17] however, these attempts to understand the phenomenon tended to be rather qualitative. A quantitative theory for flexible polymers with a predictive power which can explain the measured profiles of the mean velocity as a function of the distance from the wall was achieved only recently.[18,19] For rodlike polymers, the stress tensor $\boldsymbol{\sigma}$ takes the form:[20]

$$\sigma_{ab} = 6\nu_p n_a n_b (n_i n_j S_{ij}), \tag{5}$$

where ν_p is the viscosity contributed by the polymer in the limit of zero shear, $\boldsymbol{n}\equiv\boldsymbol{n}(\boldsymbol{r},t)$ is a unit vector describing the orientation of the polymer, and $S_{ij}\equiv\partial U_i/\partial r_j$ is velocity gradient. The equation of motion for the orientations of the polymers is approximated by the rigid-dumbbell model which reads

$$\frac{D\mathcal{R}_{ab}}{Dt} = S_{ai}\mathcal{R}_{ib} + S_{bi}\mathcal{R}_{ia} - 2S_{ij}\mathcal{R}_{ij}\mathcal{R}_{ab} - 6\gamma\left(\mathcal{R}_{ab} - \frac{\delta_{ab}}{3}\right), \tag{6}$$

where $\mathbf{R}\equiv\boldsymbol{nn}$ and γ is the Brownian rotational frequency, proportional to temperature.

A. High Re flows

The phenomenon of drag reduction in highly turbulent channel flows can be understood on the basis of the balance equations of the mechanical momentum and turbulent energy.[18] For a channel flow, we choose the coordinates x, y, and z as the lengthwise, wall-normal, and spanwise directions, respectively. The length and width of the channel are usually taken much larger than the midchannel height L, making the latter a natural rescaling length for the introduction of dimensionless (similarity) variables, also known as "wall units."[21] By denoting the pressure gradient

$p' \equiv -\partial p/\partial x$, we define the friction Reynolds number Re_τ, the normalized distance from the wall y^+, and the normalized mean velocity $V^+(y^+)$ (which is in the x direction with a dependence on y only) by

$$\mathrm{Re}_\tau \equiv L\sqrt{p'L}/\nu_0, \quad y^+ \equiv y\,\mathrm{Re}_\tau/L, \quad V^+ \equiv V/\sqrt{p'L}. \tag{7}$$

The balance equations are derived on the basis of the Reynolds decomposition

$$U_i(\boldsymbol{r},t) = V(y)\delta_{ix} + u_i(\boldsymbol{r},t), \tag{8}$$

$$S_{ij}(\boldsymbol{r},t) = S(y)\delta_{ix}\delta_{jy} + s_{ij}(\boldsymbol{r},t). \tag{9}$$

In addition to the mean shear $S(y)$, we need to introduce the mean turbulent kinetic energy $K \equiv \langle u^2\rangle/2$ and the Reynolds stress $W \equiv -\langle u_x u_y\rangle$. The momentum balance equation is obtained by averaging Eq. (4) and integrating with respect to y, ending up with the exact equation,

$$\nu_0 S + W + \langle\sigma_{xy}\rangle = p'(L-y). \tag{10}$$

The physical meaning of this equation is transparent: the momentum generated by the fixed pressure gradient $p'(L-y)$ is transported to the wall by the momentum flux (Reynolds stress) W and dissipated by the Newtonian viscosity $\nu_0 S$. We will see below that the mean stress induced by the polymer ($\langle\sigma_{xy}\rangle$) is positive definite and, therefore, is an additional mechanism of dissipation due to the polymers.

In wall units, Eq. (10) can be written in the form

$$S^+ + W^+ + \langle\sigma^+_{xy}\rangle = (1 - y^+/\mathrm{Re}_\tau), \tag{11}$$

where $S^+ \equiv \nu_0 S/(p'L)$, $W^+ \equiv W/(p'L)$, and $\sigma^+_{ij} \equiv \sigma_{ij}/(p'L)$. When y^+ is not too large, e.g., in the log layer, we neglect the second term on the right-hand side (RHS), approximating the RHS as unity.

The balance equation for the turbulent kinetic energy is calculated by taking the dot product of the fluctuation part of Eq. (4) with $\mathbf{u}$,

$$WS = \frac{\partial}{\partial y}\langle u_y u^2 + u_y p - \sigma_{iy}u_i\rangle + \nu_0\langle s_{ij}s_{ij}\rangle + \langle\sigma_{ij}s_{ij}\rangle. \tag{12}$$

Also this equation is exact. We simplify it by noting that the first term on the RHS involves the spatial flux of turbulent energy. It is well-known that in the Newtonian case, this term is negligible in the log layer.[21] It was also shown that this term is negligible near the MDR simply because $K \to 0$ near the MDR. As we expect K to decrease with any amount of drag reduction, it is safe to assume that the spatial flux is still negligible also with the polymer added compared to the terms discussed next. This assumption had been verified by direct numerical simulations in Ref. 22. The second term on the RHS represents the Newtonian dissipation which is modeled (in wall units) as[18]

$$\langle s^+_{ij}s^+_{ij}\rangle \approx K^+\left(\frac{a}{y^+}\right)^2 + b\frac{(K^+)^{3/2}}{y^+}, \tag{13}$$

where a and b are dimensionless coefficients of the order of unity and $s^+_{ij} \equiv \nu_0 s_{ij}/(p'L)$ and $K^+ \equiv K/(p'L)$. The physical reasons of this model are as follows: When y^+ is small, the dissipation of the turbulent energy is dominated by the viscosity (the first term). When y^+ is large, an eddy with size y^+ and energy $K^+(y)$ loses its energy in the time scale of $y^+/\sqrt{K^+}$, which is the eddy turnover time scale. We note that the summation sign in Eq. (13) is merely a pseudosum. It only means that when y^+ is small (large), the first (second) term is more important. Writing in wall unit, Eq (12) becomes

$$W^+S^+ \sim a^2\frac{K^+}{(y^+)^2} + b\frac{(K^+)^{3/2}}{y^+} + \langle\sigma^+_{ij}s^+_{ij}\rangle. \tag{14}$$

Finally, we quote the experimental fact that in the log layer, W^+ and K^+ are proportional to each other,

$$K^+c^2 = W^+. \tag{15}$$

Experimentally, it was found that $c \approx 0.5$ in the Newtonian case and $c \approx 0.25$ in the MDR.

To estimate the polymer term on the left hand-side of Eq. (11), we first observe that for large Re when the rodlike polymers are efficiently aligned by the flow, $R_{xx} \approx 1$. Therefore, from Eq. (5), we conclude that

$$\sigma_{xy} \sim \nu_p R_{yy} S. \tag{16}$$

In wall units, the momentum equation reads

$$(1 + \nu^+_p R_{yy})S^+ + W^+ = 1 - \frac{y}{\mathrm{Re}_\tau}, \tag{17}$$

where $\nu^+_p \equiv \nu_p/\nu_0$. Note that $\nu^+_p R_{yy}$ is positive definite, showing that the contribution to the stress tensor of the rodlike polymers is, indeed, positive definite as stated above, always adding to the effective viscosity. We also stress that the notion of effective viscosity here does not mean that we disregard orientational dynamics; the point is that R_{yy} *acts* as the main component vis-a-vis the polymeric stress tensor.

To estimate the polymer term in the RHS of Eq. (12) (the energy dissipation due to the polymers), we use the results of Ref. 23 where it was shown that

$$\langle\sigma_{ij}s_{ij}\rangle \sim \nu_p R_{yy}\frac{K}{y^2}. \tag{18}$$

Putting into Eq. (12) and writing in wall unit, we have

$$W^+S^+ \sim a^2(1 + \nu^+_p R_{yy})\frac{K^+}{(y^+)^2} + b\frac{(K^+)^{3/2}}{y^+}. \tag{19}$$

Equations (17) and (19) imply that the polymers change the properties of the flows by replacing the viscosity by

$$\nu_{\mathrm{eff}} = 1 + \nu^+_p R_{yy}. \tag{20}$$

This means that polymeric flows can be reasonably described by the changing the "effective viscosity" of the solution. In the fully developed turbulent flow, it was shown in Ref. 23 that R_{yy} depends on K^+ and S^+,

$$R_{yy} = \frac{K^+}{(y^+S^+)^2}. \tag{21}$$

It was argued in Ref. 23 that for large Re, K^+ grows linearly with y^+ and, thus, the viscosity profile is linear. Furthermore, it was shown theoretically in Ref. 24 that if the effective viscosity varies linearly with y^+, i.e.,

$$\nu_{\text{eff}} = 1 + \alpha(y^+ - y_\nu^+), \tag{22}$$

then c must satisfy the relation

$$\frac{a}{c} = \frac{\delta}{1 - \alpha\delta}. \tag{23}$$

Here, $\delta \approx 6$ is the width of the viscous sublayer in the Newtonian flows.

For a given ν_{eff}, Eqs. (15), (17), (19), and (23) form a complete set of equations for variables S^+, W^+, K^+, and c. This model has been studied extensively for Newtonian flows[25] and for the flows with linear viscosity profile.[24] The resulting velocity profiles agree reasonably with the experimental results. It was found that in the viscous sublayer, the model does allows for a solution that is turbulent and, therefore, $K^+ = W^+ = 0$ and $S^+ = 1$. This also agrees quite well with existing experimental data. Moreover, an edge solution for $\alpha = 1/12$ was observed.[24] If $\alpha > 1/12$, the model no longer has a solution corresponding to a turbulent flow and, therefore, the flow must be laminar. The special case of $\alpha = 1/12$ was identified as the MDR of the polymeric drag reduction.

B. Low Re flows

According to Eq. (20), the value of ν_{eff} depends on ν_p^+ and R_{yy}. The value of ν_p^+ is determined by the polymer properties such as the number of monomers, their concentration, etc., and thus, ν_p^+ should be considered as an external parameter in the equation. The value of R_{yy}, on the other hand, depends on the properties of the flow. In the case of laminar flow with a constant shear rate, i.e., $K^+ = W^+ = 0$ and $S^+ =$ constant, it was shown theoretically in Ref. 20 that

$$R_{yy} = \frac{2^{1/3}}{\text{De}^{2/3}}, \tag{24}$$

where the Deborah number De is defined by $\text{De} = S/\gamma$. Thus, the effective viscosity is reduced if S is increased and, therefore, the rodlike polymers solution is a shear-thinning liquid. Naturally, The value of De changes with Re. To clarify this dependence, we consider the momentum equation [Eq. (10)] at $y = 0$ in the Newtonian case,

$$\nu_0 S = p'L. \tag{25}$$

Usually in experiments, system size and the working fluid remain to be the same. Therefore, ν_0 and L are constants and so, Re_τ depends on $p'L$ only. According to Eq. (7), Re_τ grows as $\sqrt{p'L}$, and therefore,

$$\text{De} = \frac{\nu_0}{\gamma L^2}\,\text{Re}_\tau^2 \tag{26}$$

by Eq. (25). Putting into Eq. (24), we have

$$\nu_{\text{eff}} = 1 + \nu_p^+ \frac{\lambda}{\text{Re}_\tau^{4/3}}, \tag{27}$$

where $\lambda \equiv \nu_0/\gamma L^2$ is a constant.

C. Intermediate Re flows

In the case of intermediate Re, we need an interpolation between Eqs. (21) and (24). To do this, we note that when y^+ is small, the solution of Eqs. (15), (17), and (19) result in $W^+ = K^+ = 0$ in the viscous sublayer. This implies that the flow cannot be highly turbulent in the viscous sublayer. Thus, it is reasonable to employ Eq. (24) as long as y^+ is small. On the other hand, as the upper bound of y^+ is Re_τ, when y^+ is large, it automatically implies that Re_τ is large. The laminar contribution is, therefore, negligible as it varies inversely with Re_τ. The effective viscosity due to the polymer is dominated by the turbulent estimate [Eq. (21)]. To connect these two regions, we simply use the pseudosum,

$$\nu_{\text{eff}} = 1 + \nu_p^+ \left[\frac{\lambda}{\text{Re}_\tau^{4/3}} + \frac{K^+}{(y^+S^+)^2} \right] = g + \nu_p^+ \frac{K^+}{(y^+S^+)^2}, \tag{28}$$

where $g \equiv 1 + \nu_p^+ \lambda / \text{Re}_\tau^{4/3}$. One can see that the limits for both high and low Re_τ are satisfied.

IV. SOLUTION AND RESULTS

A. Setting up the equations

Having the expression for ν_{eff}, we have to specify the value of c in Eq. (15) to complete the equations. This variable naturally depends on α and g. The latter dependence, however, can be eliminated by rescaling the dimensional variables. Define

$$\tilde{\text{Re}}_\tau \equiv \frac{L\sqrt{p'L}}{g\nu_0}, \quad \tilde{y}^+ \equiv \frac{y\,\tilde{\text{Re}}_\tau}{L}, \quad V^+ \equiv \frac{V}{\sqrt{p'L}}. \tag{29}$$

In these units, Eq. (28) is written as

$$\tilde{\nu}_{\text{eff}} = 1 + \tilde{\nu}_p \frac{\tilde{K}^+}{(\tilde{y}^+\tilde{S}^+)^2}, \tag{30}$$

where $\tilde{\nu}_p = \nu_p/g$, $\tilde{S}^+ = S^+ g$, and $\tilde{K}^+ = K^+$. We can find the α dependence by comparing Eq. (30) to Eq. (22) and identifying the width of the viscous sublayer $\tilde{y}_\nu^+$ with $a/c(\alpha)$. This stems from the continuity of $\tilde{S}^+$ at the boundary of the viscous sublayer. This means that

$$a/c(\alpha) = \tilde{y}_\nu^+. \tag{31}$$

Combining Eqs. (22), (23), and (31), the relationship between $\tilde{\nu}_{\text{eff}}$ and c is

$$\tilde{\nu}_{\text{eff}} = 1 + \frac{a - c\delta}{a\delta}\left(\tilde{y}^+ - \frac{a}{c}\right). \tag{32}$$

We note also that Eqs. (22) and (30) can be written as

$$\tilde{K}^+ = A^2(\tilde{S}^+\tilde{y}^+)^2, \tag{33}$$

with

$$A^2 = \frac{\tilde{\nu}_{\text{eff}} - 1}{\tilde{\nu}_p}. \tag{34}$$

By using Eqs. (15) and (33), we can rewrite Eqs. (17) and (19) as two equations for the two variables $\tilde{\nu}_{\text{eff}}$ and $\tilde{S}^+$,

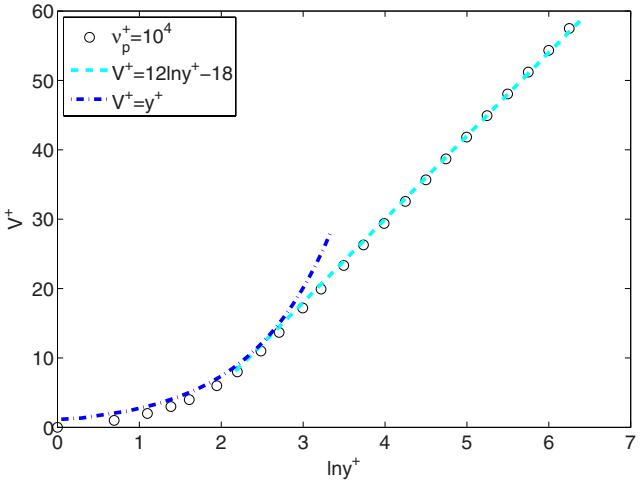

FIG. 5. (Color online) The velocity profile as predicted by the model with $\nu_p^+=10^4$ and $\mathrm{Re}_\tau=590$.

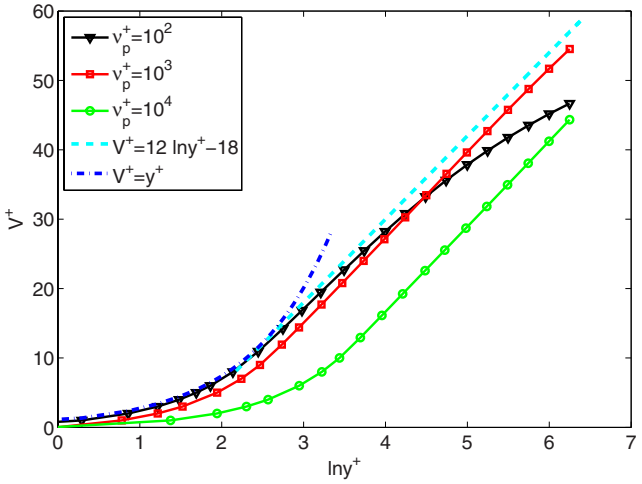

FIG. 6. (Color online) The velocity profile predicted by the model with $\mathrm{Re}_\tau=590$ and $\lambda=1$ for various values of ν_p^+.

$$\tilde{\nu}_{\mathrm{eff}}\tilde{S}^+ + c^2A^2(\tilde{S}^+\tilde{y}^+)^2 = 1 \tag{35}$$

and

$$c^2\tilde{S}^+ = \tilde{\nu}_{\mathrm{eff}}\left(\frac{a}{\tilde{y}^+}\right)^2 + bA\tilde{S}^+. \tag{36}$$

Equation (36) implies that

$$\tilde{S}^+ = \frac{\tilde{\nu}_{\mathrm{eff}}}{(\tilde{y}^+)^2}\frac{a^2}{(c^2-bA)}. \tag{37}$$

Substituting Eq. (37) into Eq. (35) gives an equation for ν_{eff},

$$\tilde{\nu}_{\mathrm{eff}}^2\left(\frac{a}{\tilde{y}^+}\right)^2(c^2-bA) + c^2A^2\tilde{\nu}_{\mathrm{eff}}^2\left(\frac{a^2}{\tilde{y}^+}\right)^2 = (c^2-bA)^2. \tag{38}$$

Finally, we can solve Eqs. (32) and (38) to get $\tilde{\nu}_{\mathrm{eff}}(y^+)$ for different values of $\tilde{\nu}_p$. Then, we can obtain $\tilde{S}^+$ and $\tilde{K}^+$ by using Eqs. (33) and (37), respectively. Finally, we reexpress the variables in wall unit by using Eq. (29).

B. Comparison of analysis with experiments

To compare our analytical results with the experiments, we first solve the model with Eq. (28) for $\mathrm{Re}_\tau=590$ and for $\lambda=0$, i.e., the high Re limit. This demonstrates that the MDR is reproduced within the model, as shown in Fig. 5.

We observe that V^+ is increasing with a constant rate for small y^+ and then follows the log law of the MDR. The results for $\lambda=1$ are shown in Fig. 6. We note that for $\nu_p^+=100$, the velocity profile first follows the viscous profile and then joins the MDR until it begins to cross back to the Newtonian plug. For $\nu_p^+=1000$, the viscous layer is increased in size, but then the velocity profile becomes parallel to the MDR but with a smaller intercept, signaling less efficicient drag reduction. Once ν_p^+ reaches the value of 10 000, the viscous layer becomes rather large, of the order of 20. The velocity profile still succeeds to run parallel the MDR but with a much reduced intercept.

To compare the prediction of the model to the experimental results shown in Fig. 1, we need to relate Re_τ to Re as used in that figure. The relation is

$$\mathrm{Re}_L \equiv Re_\tau V_L^+, \tag{39}$$

where V_L^+ is the velocity at the center of the channel. Figure 7 shows $f^{-1/2}$ as a function of $\log_{10}(\mathrm{Re}_L f^{1/2})$ with various values of ν_p^+. One can see that for large ν_p^+, we obtain a drag enhancement when Re_L is small. This enhancement decreases with increasing Re_L, and eventually for large enough Re_L, there is drag reduction. The maximum amount of drag reduction, however, cannot exceed the MDR. For small ν_p^+, the drag enhancement is nearly unnoticeable. However, drag reduction in this case is smaller for large Re_L because the Newtonian plug occurred earlier. It should be noted that the curves in Fig. 7 exhibit the "ladder" characteristics for different values of ν_p^+. This was identified as "type B" drag reduction by Virk *et al.*[4] and is the fundamental characteristic of drag reduction by rodlike polymers. We see that our re-

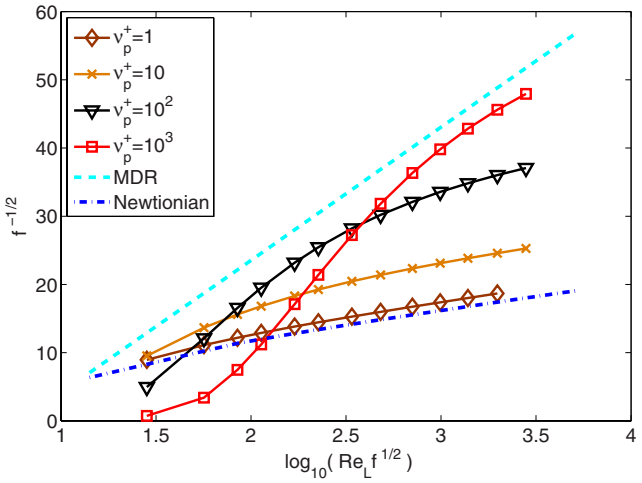

FIG. 7. (Color online) $f^{-1/2}$ as the function of $\log_{10}(\mathrm{Re}\,f^{1/2})$ with $\lambda=1$ with various values of ν_p.

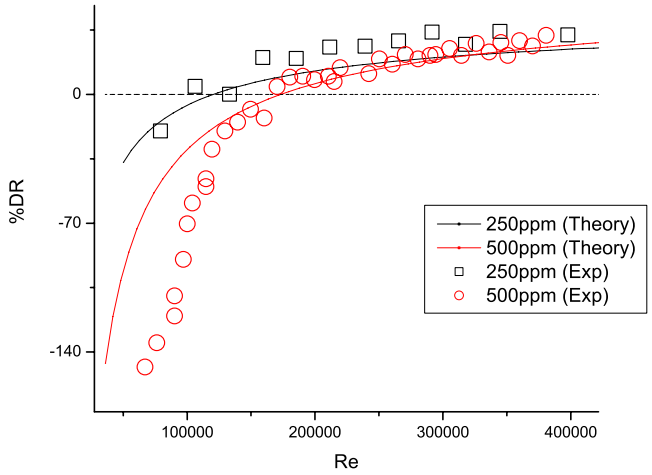

FIG. 8. (Color online) % DR as a function of the Reynolds number. The experimental results are drawn from Fig. 3 and the theoretical results from solving the model in Sec. IV B.

sults agree reasonably well with the experiments presented in Prandtl–Kármán coordinates.

To compare the theory to the experimental results in DR(%) versus Re coordinates, we use the experimentally measured values of g and ν_p to predict the amount of drag reduction. As we mentioned before, the effective viscosity in laminar flow of xanthan gum (XG) solutions is well approximated by Ostwald–de Waele model. This implies that in the low-Re flow, g is given by (in MKS units),

$$g = k_1 S^{n-1} = k_1 \left(\frac{\nu_0 \mathrm{Re}_\tau^2}{L^2} \right)^{n-1}, \tag{40}$$

where the last equality is obtained by multiplying Eq. (26) by γ. The experimental value of ν_p for XG solution is given by (in MKS units)

$$\nu_p = 0.011\,147 C^{1.422} \nu_0, \tag{41}$$

where C is the concentration of XG in wppm. The value of f can then be calculated by (i) obtaining the experimental values of C, k_1, and n for Eqs. (40) and (41), (ii) rescaling the variables S, K, and W by Eq. (29), and finally, (iii) solving Eqs. (32) and (38) to get f as a function of Re_L. It should be noted that in the present experiments, the definition of Reynolds number is, in general, different from our definition in Eq. (39). For the sake of comparison of the theory with the experiments, we assert that two Reynolds numbers must be proportional to each other. The easiest way to find the proportionality factor is to compare the point of transition from drag enhancement to drag reduction for a given polymer concentration (making sure that this ratio of proportionality does not depend on the polymer concentration). The result of this is the relation

$$12\mathrm{Re}_L \approx \mathrm{Re}_{\mathrm{exp}}. \tag{42}$$

Figure 8 shows the comparison of the percentage of drag reduction (enhancement) between the theoretical predictions and the experimental results. The two data sets shown pertain to $c=250$ wppm ($k_1=11.04$, $n=0.727$) and $c=500$ wppm ($k_1=40.62$, $n=0.607$). The agreement between theory and experiment is very satisfactory. We reiterate that in the comparison of theory and experiment, there is no free parameter employed, all the constants were measured directly in the experimental apparatus as explained above.

V. DISCUSSION AND CONCLUSIONS

In summary, we studied the Re dependence of the drag reduction by rodlike polymers. We showed that when the value of Re is small, the drag is *enhanced* due to the homogenous increase in the effective viscosity. When Re is sufficiently large, due to the turbulent activity, the effective viscosity varies as a function of the distance to the wall. As the result, the amount of drag is reduced. We use a simple interpolation between low Re and the high Re flows to account for this. The resulting theoretical results agree semiquantitatively with the experiments both in Prandtl–Kármán coordinates and in DR(%) versus Re coordinates.

It should be noted that only rodlike polymers exhibit drag enhancement for low Re. For flexible polymers, the drag is the same as that of the Newtonian flow for low Re, and only after a critical value of Re, the drag reduction sets in.[2,26] This difference in behavior from rodlike polymers is because the flexible polymers are coiled when Re is small. They do not affect the flow unless Re increases enough to allow the shear to develop to affect the coil-to-stretch transition in the flexible polymers. In contrast, rodlike polymers are always extended and, therefore, they can affect the flow for all Re.

We note that in this paper, the theory had been employed to understand the mean velocity and percent drag reduction only, but the same theory can also provide without further experimental input the profiles of Reynolds stress and kinetic energy. For such comparisons of theory with numerical simulation, the reader is referred to Ref. 22.

ACKNOWLEDGMENTS

This work has been supported in part by the European Commission under a TMR grant and by the US-Israel Bi-National Science Foundation.

[1] B. A. Toms, *Proceedings of the First International Congress in Rheology Amsterdam* (North-Holland, Amsterdam, 1948), Vol. 2, p. 135.
[2] P. S. Virk, "Drag reduction fundamentals," AIChE J. **21**, 625 (1975).
[3] A. Gyr and H. W. Bewersdorff, *Drag Reduction of Turbulent Flows by Additives* (Kluwer, London, 1995).
[4] P. S. Virk, D. L. Wagger, and E. Koury, "The asymptotic maximum drag reduction induced by additives in internal flows," FED (Am. Soc. Mech. Eng.) **237**, 261 (1996).
[5] C. Wagner, Y. Amarouchene, P. Doyle, and D. Bonn, "Turbulent-drag reduction of polyelectrolyte solutions: Relation with the elongational viscosity," Europhys. Lett. **64**, 823 (2003).
[6] O. Cadot, D. Bonn, and S. Douady, "Turbulent drag reduction in a closed flow system: Boundary layer versus bulk effects," Phys. Fluids **10**, 426 (1998).
[7] O. Cadot, Y. Couder, A. Daerr, S. Douady, and A. Tsinober, Phys. Rev. E **56**, 427 (1997).
[8] C. A. Kim, H. J. Choi, C. B. Kim, and M. S. Jhon, "Drag reduction characteristics of polysaccharide xanthan gum," Macromol. Rapid Commun. **19**, 419 (1998).
[9] A. S. Pereira and F. T. Pinho, "Turbulent characteristics of shear-thinning fluids in recirculating flows," Exp. Fluids **28**, 266 (2000).

[10]J.-I. Sohn, C. A. Kim, H. J. Choi, and M. S. Jhon, "Drag reduction effectiveness of xantan gum in a rotating disk apparatus," Carbohydr. Polym. **45**, 61 (2001).
[11]R. B. Bird, R. C. Armstrong, and O. Hassager, *Dynamics of Polymeric Liquids* (Wiley, New York, 1987), Vols. 1 and 2.
[12]A. Lindner, D. Bonn, E. Corvera Poire, M. Ben Amar, and J. Meunier, "Viscous fingering in non-Newtonian fluids," J. Fluid Mech. **469**, 237 (2002).
[13]A. V. Bazilevskii, S. I. Voronkov, V. M. Entov, and A. N. Rozhkov, "Orientational effects in the decomposition of streams and strands of diluted polymer solutions," Sov. Phys. Dokl. **26**, 333 (1981); S. L. Anna and G. H. McKinley, "Elasto-capillary thinning and breakup of model elastic liquids," J. Rheol. **45**, 115 (2001); Y. Amarouchene, D. Bonn, J. Meunier, and H. Kellay, "Inhibition of the finite-time singularity during droplet fission of a polymeric fluid," Phys. Rev. Lett. **86**, 3558 (2001).
[14]F. T. Trouton, "On the coefficient of viscous traction and its relation to that of viscosity," Philos. Mag. **19**, 347 (1906).
[15]M. T. Landahl, "Dynamics of boundary layer turbulence and the mechanism of drag reduction," Phys. Fluids **20**, S55 (1977).
[16]J. L. Lumley, "Drag reduction in two phase and polymer flows," Phys. Fluids **20**, S64 (1977).
[17]H.-W. Bewersdorff and N. S. Bergman, "The influence of flow-induced non-Newtonian fluid properties on turbulent drag reduction," Rheol. Acta **27**, 130 (1988).
[18]V. S. L'vov, A. Pomyalov, I. Procaccia, and V. Tiberkervich, "Drag reduction by polymers in wall bounded turbulence," Phys. Rev. Lett. **92**, 244503 (2004).
[19]I. Procaccia, V. S. L'vov, and R. Benzi, "Colloquium: Theory of drag reduction by polymers in wall bounded turbulence," Rev. Mod. Phys. **80**, 225 (2008).
[20]M. Doi and S. F. Edwards, *The Theory of Polymer Dynamics* (Oxford University Press, Oxford, 1988).
[21]S. B. Pope, *Turbulent Flows* (Cambridge University Press, Cambridge, 2000).
[22]R. Benzi, E. S. C. Ching, E. de Angelis, and I. Procaccia, "Comparison of theory and direct numerical simulations of drag reduction by rodlike polymers in turbulent channel flows," Phys. Rev. E **77**, 046309 (2008).
[23]R. Benzi, E. S. C. Ching, T. S. Lo, V. S. L'vov, and I. Procaccia, "Additive equivalence in turbulent drag reduction by flexible and rodlike polymers," Phys. Rev. E **72**, 016305 (2005).
[24]R. Benzi, E. de Angelis, V. S. L'vov, and I. Procaccia, "Identification and calculation of the universal maximum drag reduction asymptote by polymers in wall bounded turbulence," Phys. Rev. Lett. **95**, 194502 (2005).
[25] V. S. L'vov, A. Pomyalov, and V. Tiberkevich, "Simple analytical model for entire turbulent boundary layer over flat plane," Environ. Fluid Mech. **5**, 373 (2005).
[26]D. Bonn, Y. Amarouchene, C. Wagner, S. Douady, and O. Cadot, "Turbulent drag reduction by polymers," J. Phys.: Condens. Matter **17**, S1195 (2005).